Mosquito bite prevention through graphene barrier layers

Cintia J. Castilho[a], Dong Li[a], Muchun Liu[a,b], Yue Liu[a], Huajian Gao[a,1], and Robert H. Hurt[a,1]

[a]School of Engineering, Brown University, Providence, RI 02912; and [b]Department of Chemistry, Brown University, Providence, RI 02912

Contributed by Huajian Gao, July 23, 2019 (sent for review April 17, 2019; reviewed by Mathew Begley and Yuan Chen)

Graphene-based materials are being developed for a variety of wearable technologies to provide advanced functions that include sensing; temperature regulation; chemical, mechanical, or radiative protection; or energy storage. We hypothesized that graphene films may also offer an additional unanticipated function: mosquito bite protection for light, fiber-based fabrics. Here, we investigate the fundamental interactions between graphene-based films and the globally important mosquito species, *Aedes aegypti*, through a combination of live mosquito experiments, needle penetration force measurements, and mathematical modeling of mechanical puncture phenomena. The results show that graphene or graphene oxide nanosheet films in the dry state are highly effective at suppressing mosquito biting behavior on live human skin. Surprisingly, behavioral assays indicate that the primary mechanism is not mechanical puncture resistance, but rather interference with host chemosensing. This interference is proposed to be a molecular barrier effect that prevents *Aedes* from detecting skin-associated molecular attractants trapped beneath the graphene films and thus prevents the initiation of biting behavior. The molecular barrier effect can be circumvented by placing water or human sweat as molecular attractants on the top (external) film surface. In this scenario, pristine graphene films continue to protect through puncture resistance—a mechanical barrier effect—while graphene oxide films absorb the water and convert to mechanically soft hydrogels that become nonprotective.

graphene barriers | wearable technologies | mosquito bite prevention

Graphene is being explored as an enabling component in wearable fabric-based or on-skin technologies for environmental sensing (1, 2), biomonitoring (3, 4), UV protection (5), Joule heating (2), ballistic protection (6), chemical toxicant rejection (7), flame suppression (8), and energy storage (2, 9). Graphene films are ultrathin, ultralight, and electrically conductive, and textured versions can show programmed unfolding that mimics elasticity to match stretchable fabrics (2, 10). Films formed from graphene oxide (GO) nanosheets show high water-vapor transmission and thus may provide chemical protection while maintaining fabric breathability for perspiration loss and improved body heat regulation (7).

An unexplored function of graphene-based wearables is insect bite protection. Female mosquitos require blood meals in addition to plant-based foods and serve as vectors for malaria, dengue fever, yellow fever, and the chikungunya, Zika and West Nile viruses, causing infectious diseases responsible for hundreds of thousands of human deaths and hundreds of millions of nonlethal diseases annually worldwide (11). The mosquito proboscis is a highly sophisticated biting apparatus that consists of a penetrating fascicle imbedded in a protective sheath (labium) that is withdrawn during biting and serves as an insertion guide (12–14). The fascicle itself is bundle of 6 stylets, or microneedles, that act in coordinated fashion to pierce and saw through skin tissue to reach underlying blood vessels, inject anticoagulant, and remove blood (14). Mosquitoes are known to bite through light fiber-based fabrics and even some fully dense polymer films (*SI Appendix*, Fig. S7). The net forces of mosquito biting in human skin are low [measured at ~18 μN (15)], prompting researchers to use the mosquito fascicle as inspiration for the design of biomimetic microneedles for painless drug injection (13) or neural microelectrodes (12).

There is great interest in alternatives to current chemical approaches to mosquito-protective clothing and uniforms. Graphene films are fully dense 2D structures that may serve as barriers to prevent mosquito fascicle penetration, but there have been no experimental studies of graphene–mosquito interactions to assess the concept or design the films. Atomic force microscope (AFM) tips penetrate graphene or GO monolayers at forces from 80 nN to 3 μN (16–18), which are lower than the measured mosquito bite force (18 μN), suggesting monolayer graphene may not be a sufficient mechanical barrier for bite protection. We are not aware of any measurements of puncture resistance for the multilayer films commonly used in wearable technologies. Because of the biomechanical sophistication of the mosquito fascicle, we chose whole-animal live mosquito experiments on living human skin patches to directly and reliably assess mosquito–graphene interactions and the intrinsic ability of these films to inhibit biting behavior. We supplement these primary data with mechanical needle penetration measurements, mathematically modeling, and measurements of molecular permeation through the graphene films to help reveal bite inhibition mechanisms.

Results and Discussion

Captivity-bred, pathogen-free females of the species *Aedes aegypti* were contained in a glove box modified to allow human arm insertion with skin patch exposure (*Methods* and *SI Appendix*,

Significance

The mosquito is the world's most important vector for transmission of infectious diseases, and chemical agents now used for bite prevention can have environmental or human health side effects. This work explores a nonchemical method for mosquito bite prevention based on graphene, the atomically thin sheet of carbon atoms, as a potential barrier material. We show that multilayer graphene films in the dry state completely inhibit biting by preventing mosquitos from sensing skin- or sweat-associated chemicals used to locate blood meals. In some cases, the graphene films also act as mechanical barriers to the penetration of the mosquito fascicle, its feeding apparatus. The results can guide development of graphene protective technologies on skin or within smart fabrics.

Author contributions: C.J.C., D.L., M.L., Y.L., H.G., and R.H.H. designed research; C.J.C., D.L., M.L., Y.L., and R.H.H. performed research; C.J.C., D.L., M.L., Y.L., H.G., and R.H.H. analyzed data; and C.J.C., D.L., M.L., Y.L., H.G., and R.H.H. wrote the paper.

Reviewers: M.B., University of California, Santa Barbara; and Y.C., University of Sydney.

The authors declare no conflict of interest.

[1]To whom correspondence may be addressed. Email: huajian_gao@brown.edu or robert_hurt@brown.edu.

This article contains supporting information online at www.pnas.org/lookup/suppl/doi:10.1073/pnas.1906612116/-/DCSupplemental.

Published online August 26, 2019.

Fig. S3). *A. aegypti* is a daytime-biting anthropophilic mosquito [i.e., preferring humans to other animals (11)] and is an important vector for infectious diseases that include dengue fever, yellow fever, and Zika virus (11). Rectangular skin patches of typical area 4 to 6 cm^2 were exposed for 5-min intervals to batches of ∼100 mosquitos in the enclosure while being monitored by video microscopy and macrophotography (Fig. 1). Mosquito behavior (landings, residence times, head positions indicating penetration [Fig. 1*A*, yellow arrow], and abdominal swelling/red coloration indicating blood feeding [Fig. 1*A* yellow arrow]) were observed for bare and graphene-coated skin patches. Bite numbers were determined by postexposure skin examination (Fig. 1*C*) confirmed by video review of head positions and abdominal swelling. Cheesecloth (a thin, loose-weave fabric) was used in most experiments to hold the graphene films directly against the skin and avoid interstitial air gaps that might otherwise add additional resistance to fascicle penetration (Fig. 1*B*).

Fig. 1*D* shows example raw data on bite frequency from test and control samples. Bite numbers in the standard 5-min interval range from 5 to 20 on bare skin or cheesecloth-only controls, while GO films (1 μm thickness, dry state) never allowed a bite in any experiment (Fig. 1*D*). Note that "dry state" refers to films equilibrated with laboratory room air measured at 51% relative humidity, and these films contain 21 wt % water measured by thermal desorption (*SI Appendix*, Fig. S13). Fig. 1*E* shows statistics on area-normalized bite frequency. Because the GO tests were done with cheesecloth coverings (Fig. 1*B*), the effect of graphene addition is seen in the comparison to the cheesecloth (not bare skin) control, and the bite prevention effectiveness of graphene is very clear.

The dry graphene films are observed to be perfectly protective, but live animal bite data (Fig. 1) alone do not reveal the protection mechanism. We originally hypothesized graphene would serve as a mechanical barrier to fascicle penetration, but careful observation of *Aedes* behavior on the films suggests an alternative explanation. Mosquito landings were much less frequent on graphene than on bare skin and appeared to be typical for landing behavior on other (nonhuman) surfaces present in the containment vessel. Also, after landing, the typical duration of stay appeared to be much shorter, and *Aedes* did not show the intense, active proboscis probing we observed on skin, which is reported to be the first step in biting behavior (13). We quantified these visual impressions through behavioral assays tracking visitation frequencies (landings plus walk-ons) and residence time distributions on graphene-coated skin and controls for large numbers of individual mosquitos (Fig. 2). The quantitative data in Fig. 2 confirmed our early qualitative observations, and suggest that these graphene films prevent *Aedes* from sensing the human host and thus recognizing the potential for a blood meal associated with the skin lying immediately below the graphene film.

Mosquito attraction is the result of highly evolved complex, integrated sensory system based on olfactory, temperature, humidity, and visual inputs (19, 20). It has been proposed that multiple cues are needed for effective attraction and that different cues operate at different length scales of separation from the target. For example, sensing of CO_2 locates respiration plumes for long-range target identification, followed by visual identification, sensing of body odors (skin-associated volatile organic compounds), humidity and thermal plumes closer to the human host, and finally activation of gustatory (taste) receptors that promote biting once on the skin surface (19–22).

The Fig. 2 data and the absence of active probing strongly suggest that dry graphene films inhibit biting not by mechanically rejecting the fascicle but by interfering with 1 or more local host-seeking mechanisms in *A. aegypti*. Graphene is well-known to be a highly effective molecular barrier essentially impermeable to all molecules of size down to and including helium atoms (23–25). Likewise, GO nanosheet films in the dry state also reject all molecules including helium atoms (26), and the molecular barrier fidelities of the particular films used here were assessed through permeation experiments using hexane as a standard vapor permeant (*SI Appendix*, Fig. S2). It is thus expected that the *Aedes* olfactory and gustatory receptors would not have access to skin associated molecular attractants, which are trapped beneath these impermeable graphene films and thus nonbioavailable (Fig. 2*D*).

To seek additional support for the molecular barrier hypothesis, the behavioral and bite experiments were repeated with human sweat or water on the outside surface of the graphene films (*SI Appendix*, Fig. S6). Humidity and sweat-associated organic chemicals are known mosquito attractants (19–21) that when applied externally become bioavailable to mosquito chemical receptors

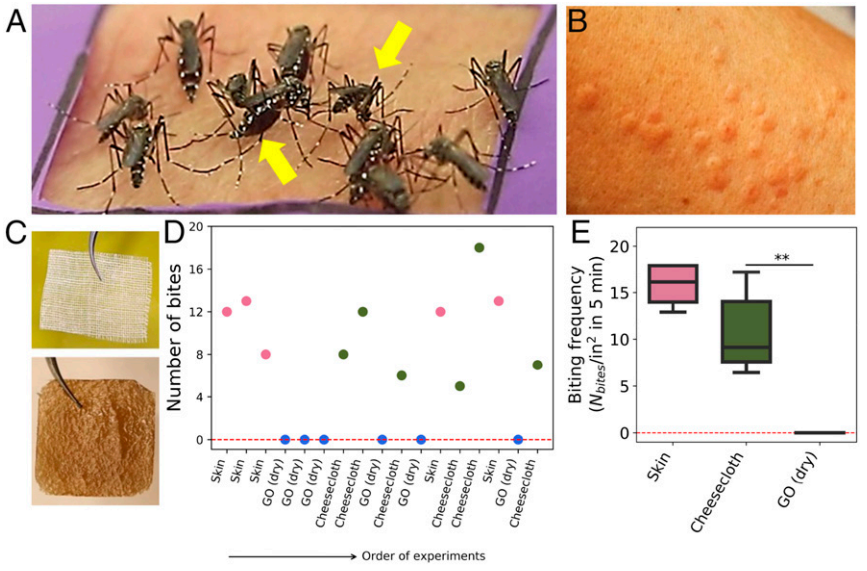

Fig. 1. Effect of graphene films (dry state) on mosquito biting behavior. (*A*) Typical *Aedes* behavior observed during bare skin control experiments with yellow arrows showing 2 bite indicators: *Left* arrow, red, swollen abdomen reflecting successful blood feeding; *Right* arrow, head-down position indicating fascicle insertion. (*B*) Skin patch following an example control experiment (no graphene), showing inflammatory reaction used as a third bite indicator. (*C*) Structures of standard cheesecloth (*Top*) and GO nanosheet film of 2 cm lateral dimension (*Bottom*). (*D*) Example raw data on bite counts (bites per 5-min experiment) presented in the order in which the randomized trials were performed. No bites were recorded during any experiment with dry GO films. (*E*) Box plot of area-normalized mosquito bite frequency on dry GO films vs. controls. Horizontal bars indicate the median, the boxed area extends from the 25th to 75th percentiles, and whiskers show the minimum to maximum range. Statistical significance was calculated using Welch's *t* test (1-tailed test). $^{**}P < 0.01$. An alternative statistical model ignores the small variations in exposed areas and treats total bite numbers as count data (positive integers) that follow a Poisson distribution model based on independent bite probabilities, λ, in a given time interval. This alternative analysis yields even lower *P* values (*SI Appendix*, Fig. S5) indicating very high confidence in the inhibiting role of dry GO films. All of the graphene films were pressed onto skin with a layer of cheesecloth to prevent air gaps.

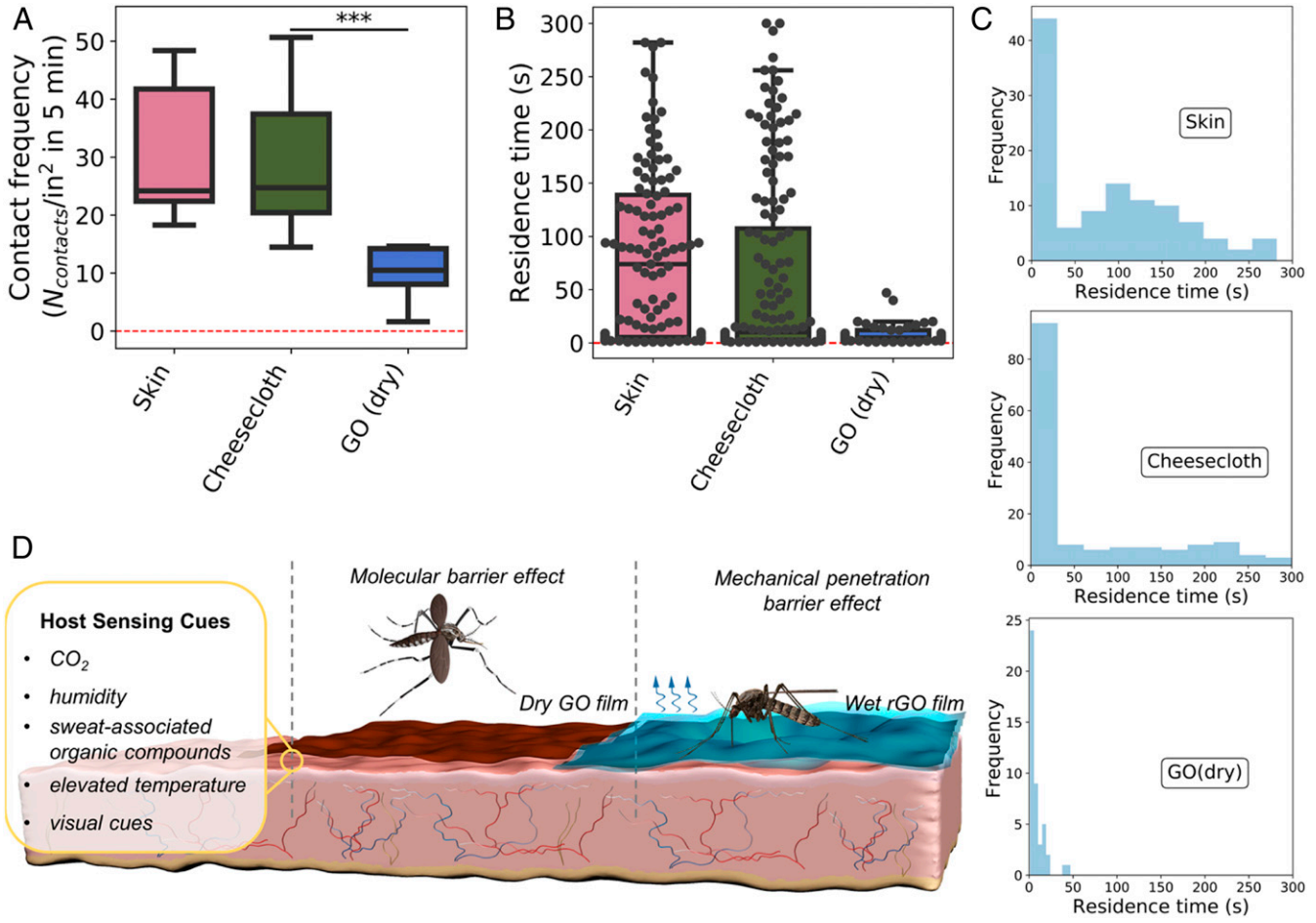

Fig. 2. Mosquito behavioral assays and mechanisms of bite inhibition. (*A*) Box plot of mosquito contact frequency (landings plus walk-ons) on dry GO films compared to controls. (*B*) Box plot of *Aedes* residence times after initial contact with dry GO films compared to controls. Black circles represent individual data points. (*C*) Residence time distributions (10 bins) of mosquitoes on skin, cheesecloth, and dry GO. (*D*) Sketch of possible bite inhibition mechanisms on dry GO and wet rGO films. (*Left*) A selection of chemical, thermal, and optical cues reported to play a role in mosquito host sensing (19, 20). Chemical cues (CO_2, humidity, and sweat-associated organic compounds) are rendered nonbioavailable by a molecular barrier effect exerted by the overlaying (nonwetted) GO films (*Center*). Addition of water or sweat as an attractant on the outer surface of graphene (rGO) films successfully attracts mosquitos (*Right*), but still prevents biting through a mechanical penetration barrier effect (Fig. 3). Box plot interpretation is the same as in Fig. 1. Statistical significance was calculated using Welch's *t* test (1-tailed test). ***$P < 0.05$. All of the graphene films were pressed onto skin with a layer of cheesecloth to prevent air gaps.

without the need for permeation through a graphene film. Fig. 3 shows that adding an excess of deionized water or fresh human sweat to the graphene films greatly increases the contact frequency of *Aedes* on GO films—even to values above those for bare skin (Fig. 3*A*)—as well as increases mean residence times (Fig. 3*C*). The ability of surface water alone to attract mosquitos in this environment can be reproduced in experiments without human skin (Fig. 3*D*). Parafilm [a polymer used in mosquito feeders as artificial skin (27, 28)] was stretched over an empty glass vessel and covered by GO films and cheesecloth. We observed a large difference in contact frequency when these films were dry vs. wet (Fig. 3*D*). *Aedes* readily lands and remains on water-covered graphene or water-soaked graphene/cheesecloth multilayers (*SI Appendix*, Fig. S4).

Having attracted *Aedes* to the target skin patch, these water/sweat experiments can provide information on the ability of graphene films to also act as mechanical barriers to fascicle penetration. In the presence of water or human sweat, we observed the mosquitos to land, stay, and actively probe but for reduced GO (rGO) films not to successfully bite (Fig. 3*B*). This suggests rGO films resist mechanical penetration of the fascicle, a conclusion that will be confirmed through needle penetration experiments and mechanical modeling (vide infra). An unexpected finding of our study was the ability of mosquitos to bite through (unreduced) GO films in the wet state (Fig. 3*B*). The bite frequencies are lower than those with cheesecloth alone but are nonzero and reproducible. Water or sweat are clearly sufficient as an attractant, and once on the surface, the *Aedes* fascicle can penetrate the 1-μm-thick GO wet films to reach human skin and underlying blood vessels. GO is known to be a hygroscopic material (29), and contacting our films with excess liquid water causes absorption, swelling, and the formation of hydrogels without the characteristic 001 XRD peak of stacked GO nanosheets in the dry state (*SI Appendix*, Figs. S13 and S14). We observe our wet GO films to be easily destroyed upon handling. In contrast, rGO films with reduced oxygen functionality do not absorb water or swell, and likely retain their mechanical properties.

We hypothesized that the different behavior of GO and rGO films under fully wet conditions reflects different degrees of mechanical resistance to mosquito fascicle penetration. This mechanical barrier hypothesis was explored using needle penetration tests and micromechanical modeling. Initial AFM studies with micro-Newton forces were unable to penetrate these multilayer graphene films (*SI Appendix*, Note 1). We then performed

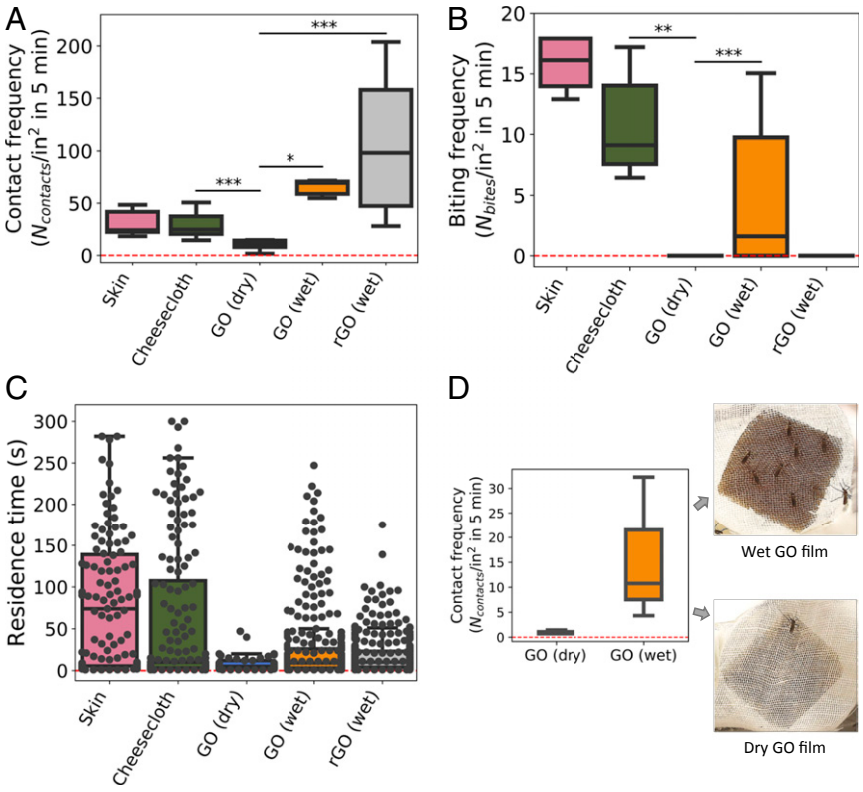

Fig. 3. Effect of water or human sweat addition to the behavior of mosquitos on graphene films. (*A*) Experimental statistics on mosquito contact frequency on dry and wet graphene films compared to control experiments. Water or human sweat (pooled data) act as attractants that greatly increase contact frequency. (*B*) Box plot of mosquito biting frequency on dry and wet graphene films compared to control experiments. *Aedes* successfully bites through wet GO but not dry GO or wet rGO. (*C*) Box plot of mosquito residence time after landing on wet and dry graphene films compared to control experiments. Black circles represent individual data points. (*D*) Nonhuman experiment to test the effect of surface water as a mosquito attractant. A 1-um GO layer was placed between stretched Parafilm and cheesecloth and exposed to mosquitoes for 5 min in the dry and wet states. Box plot definitions and statistics are the same as in Figs. 1 and 2. $*P < 0.001$; $**P < 0.01$; $***P < 0.05$.

microneedle penetration tests at milli-Newton force levels (Fig. 4 and *SI Appendix*, Fig. S8). *SI Appendix*, Fig. S8, shows the needle tip structure and example force–displacement curves, from which the critical (maximum) penetration forces were extracted (Fig. 4). Critical penetration force increases linearly with film thickness and in the dry state is similar for GO and rGO films (Fig. 4). Addition of excess liquid water has no significant effect on rGO film but greatly reduces the penetration resistance of GO film (Fig. 4). The successful biting behavior of *Aedes* through wet GO films is believed to be due to the combination of surface water/sweat as an attractant and the mechanical softness of the resulting GO hydrogels.

To help understand the mechanical response of GO–rGO films in needle penetration tests and to validate the mechanical barrier hypothesis, we adopted a continuum membrane model where a circular, elastic membrane with clamped edges is indented by a rigid sphere at the center (Fig. 4*B*). See *SI Appendix* for details and for finite element (FE) simulations that validate the continuum model (*SI Appendix*, Fig. S9).

In this study, the Young's modulus E was estimated by nonlinear fitting with needle penetration experimental data (*SI Appendix*, Fig. S12). A cubic power law between indentation force and central deflection (30, 31) can be identified in the theoretical model and then utilized for the fitting process (*SI Appendix*, Fig. S12). The average fitted Young's moduli of GO–rGO films (2.28 GPa/2.55 GPa) are lower than previously reported values (32–35) probably due to differences in GO–rGO sheet sizes, drying conditions, and reduction conditions (for rGO films). *SI Appendix*, Table S3, lists some other model parameters corresponding to the needle penetration experiment. The Poisson's ratio for GO–rGO films was taken as $\nu = 0.17$, and small deviation from the exact value had been shown having little influence on our model (*SI Appendix*, Fig. S11).

Here, we use the model to extrapolate penetration forces from the measured values for microscale needles to values expected for the submicron mosquito fascicle. From our analytical and FE results, the penetration force behaves linearly with tip radius under the same membrane strength (Fig. 4*C*). Further, the lines in Fig. 4*C* should pass through the origin considering the limit of tip radius approaching zero. The slopes of these lines can be determined from needle penetration experimental data for at least 1 tip radius. Then the insertion force of mosquito to penetrate the same membrane can be extrapolated using the tip radius of mosquito fascicle. Based on results of our needle penetration experiment, the insertion force of mosquito to penetrate a 1.0-μm-thick GO–rGO film is estimated to fall in the range of 100 to 500 μN assuming the tip radius of mosquito fascicle to be 0.1 to 0.5 μm (13). Considering the idealization of our clamped boundary condition, the real forces needed could be even larger. Since the insertion forces of mosquito to penetrate human skin are only 10 to 20 μN (15), the above calculation suggests that 1 -μm-thick GO–rGO films would prevent fascicle penetration and thus supports the mechanical barrier hypothesis.

Membrane thickness is an important parameter for designing smart fabrics against mosquito bites. Under the assumption of a thin membrane with negligible bending stiffness, the penetration force predicted from our membrane penetration model is linearly proportional to the film thickness, in agreement with the needle penetration experiments and FE simulations (Fig. 4*D*). This can be understood from the fact that the indentation force F and membrane thickness h can be grouped into a dimensionless variable $q = \frac{1}{2\pi Ea}\left(\frac{F}{h}\right)$, where a is the membrane radius. With the help of such a linear relationship and the experimental results on 1.0 -μm-thick GO–rGO films, the required force for a mosquito to penetrate a 0.5 -μm-thick film is estimated to be within 50 to 250 μN, which is still above the typical range of force that a mosquito exerts in penetrating human skin.

In some situations, GO–rGO films may be supported directly on the skin rather than freestanding. Finite element simulations (*SI Appendix*, Fig. S10) show that the penetration forces in the presence of skin support are significantly larger than that in the

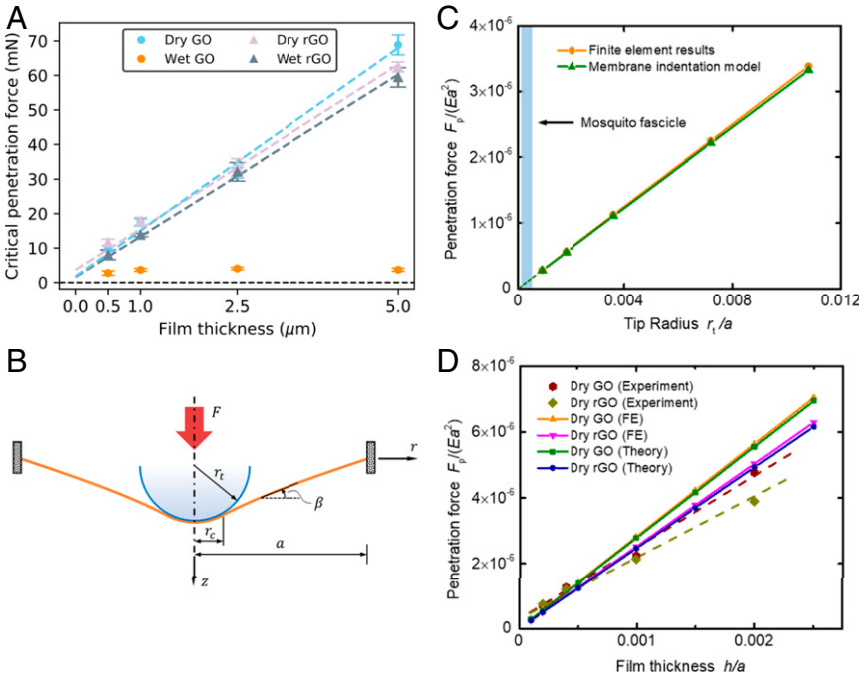

Fig. 4. Mechanical penetration resistance of various graphene films. (*A*) Measured critical penetration forces for graphene films of varying thicknesses in the dry and wet states. Data are presented as mean ± SEM ($n = 9$). (*B*) Schematic illustration of the membrane indentation model. *F* and *a* are the indentation force and membrane radius, respectively; the radii of the indenter tip and the circular contact area are denoted by r_t and r_c, respectively; and β is the local inclination angle of the membrane relative to the horizontal direction. (*C*) Linear relationships between the critical penetration force (F_p) and indenter tip size predicted from finite element and analytical models. The membrane thickness is taken as $h/a = 4 \times 10^{-4}$. (*D*) Variations of penetration force with different film thicknesses for GO–rGO films in the dry state. Dashed lines for experimental data are used for reference to show the linear relationships.

freestanding case. Therefore, the freestanding model provides a safe, lower bound design for graphene-based smart fabrics. Overall, this membrane indentation model provides theoretical support for the experimental observation that dry GO–rGO films of 0.5 to 5.0 μm thickness are sufficient mechanical barriers to mosquito fascicle insertion.

In summary, we show that graphene-based films as used in wearable technologies can provide an additional function: mosquito bite protection. In the dry state, GO and rGO films are fully protective against biting behavior, in which the primary mechanism is the interruption of the integrated host-sensing system in *A. aegypti* by concealment of skin-associated molecular attractants (e.g., CO_2, water vapor, organic compounds, and their skin microbiota metabolites) through the molecular barrier properties of graphene. In contrast, introducing liquid water or sweat on the external film surface acts as a mosquito attractant that bypasses the molecular barrier, and under these wet conditions, only those graphene films with sufficient mechanical puncture resistance offer bite protection, i.e., rGO with surface water but not GO hydrogel. We anticipate that in practice, GO hydrogels may form through contact with external sources of liquid water or through internal contact with human sweat or saturated water vapor in the skin–fabric microclimate layer under high-perspiration conditions. These results provide guidance for the design of graphene-enhanced smart fabrics for increased functionality.

Methods

Materials. Anhydrous acetone, dichloromethane (DCM), and ethanol were purchased from Sigma-Aldrich, and 55% Hydroiodic acid (HI) as a reductant was purchased from Thermo Fisher Scientific. Laboratory nitrile gloves were purchased from Kimberly-Clark Professional. Clear polystyrene substrates were purchased from Grafix. All water was deionized (18.2 MΩ, mill-Q pore). All reagents were used as received without further purification.

Fabrication of GO Nanosheet Films. GO suspensions were prepared by a modified Hummer's method as described previously (7) with nanosheet lateral size of ~1 μm, a thickness of ~1 nm (*SI Appendix*, Fig. S1), and a C/O atomic ratio of ~2.1. The concentration of stock GO suspension was about 2.5 mg mL^{-1}. The polymer substrates were cut into 9-cm^2 squares and washed with ethanol. Once dry, the squares were treated with pure oxygen plasma in a Harrick Plasma PDC-001 System to facilitate wetting. The chamber pressure was maintained at 0.13 mbar of air. Plasma was then generated at 100% power (50 W) for 30 min followed by slow venting of the chamber. Next, 650 μL of GO suspension were drop-cast onto the substrates (to make 1-um-thick films). Once dry, the polystyrene substrates were dissolved in DCM, and the detached freestanding GO films were washed with DCM, acetone, and ethanol prior to use.

Fabrication of Chemically rGO Films. The reduction was carried out by exposing the GO films to HI vapor at 85 °C for 1 to 5 min (24). The exposure time was varied according to the thickness of the film. A beaker with 2 mL of HI was heated to the specified temperature, and the films were then placed on a layer of cheesecloth on top of the beaker and exposed to HI vapor. The films were rinsed with ethanol to remove residual HI and placed to dry in an oven at 60 °C.

Graphene Film Characterization. Surface morphology of the graphene nanosheets was investigated using a field emission scanning electron microscope (SEM) (LEO 1530 VP) operating at 20.0 kV for low-, medium-, and high-resolution imaging. Before the SEM imaging, the films were coated with a layer of AuPd (~2 nm). Surface morphology and thickness of GO nanosheets were also characterized by AFM (Asylum MFP-3D Origin) operating in contact mode. The interlayer spacing of the various graphene films was measured with a Bruker AXS D8 Advance instrument with Cu KR radiation (λ = 1.5418 Å) in the dry (*SI Appendix*, Fig. S1) and dry vs. wet states (*SI Appendix*, Fig. S14). Photographs were taken with a Canon EOS Rebel T6S camera (18 to 135 mm lenses).

Live Mosquito Experiments. One hundred pathogen-free-certified female mosquitoes of species *A. aegypti* (aka the Dengue fever mosquito or the yellow fever mosquito) were purchased from Benzon Research for each batch of experiments. Cheesecloth (grade 90) was purchased from Sceng,

and mosquito traps (to manage possible mosquito escapes) were purchased from Crazo. The mosquitoes were kept inside a customized Plexiglas glovebox (89 cm width × 66 cm height × 48 cm depth). Procedures for handling live mosquitos were adapted from Imam et al. (36). The temperature was controlled to be 27 °C ± 2 °C by using a heat lamp (Byblight) and a temperature controller. The relative humidity was kept at 75 ± 5% by using a humidifier and humidity controller (*SI Appendix*, Fig. S3). The mosquitoes were subject to 12 h of light and 12 h of darkness and fed once a day with cotton balls wet with an aqueous solution of 10% wt/wt of sucrose.

The mosquito experiments were conducted by exposing live human skin patches of defined area to the interior of the mosquito containment vessel. Experiments were performed from 9 AM to 12 PM [*A. aegypti* are known to be more active during the morning (11)], with randomized sequences of tests and controls to minimize the effects of time, sequence, and feeding state on behavior. The control experiments were performed by exposing a small area (4 to 6 cm^2) of a human hand or lower forearm, with or without cheesecloth, within the containment chamber. For the test experiments, graphene films were placed on the skin patches using a cheesecloth covering to minimize air gaps, and the edges were taped to control the active area of the test (4 to 6 cm^2). Experiments with wet films were conducted by swabbing cheesecloth on sweaty human skin (following a period of exercise) or by pipette addition of nanopure water to the top of the graphene/cheesecloth patch. All of the experiments were recorded with a Canon EOS Rebel T6S camera (18 to 135 mm lenses), and all of the graphene films were inspected for pin holes and cracks using a Zeiss Stemi 2000-C optical microscope. The number of contacts (landings plus walk-ons) and residence time were extracted through frame-by-frame postanalysis of video footage. A "contact" is defined as a direct physical interaction between an individual mosquito and substrate that lasted for 1 s or longer. Bite numbers were counted in 2 ways: 1) through video observation of mosquitoes in head-down position (indicating fascicle insertion) followed by abdominal swelling and red coloration (Fig. 1*A*) and 2) by counting the inflammatory welts on the human skin after 5 to 10 min following retraction from the containment vessel (Fig. 1*C*). The study protocol was approved by Brown University's institutional review board (IRB). Volunteers were asked to sign a consent form.

Puncture Tests. The puncture tests were performed using a Mark 10 ESM303 Mechanical Test System equipped with a M5-025 series 7 1N load cell. A stainless-steel syringe needle (21 gauge) of ∼9-μm tip radius was attached to the load cell. The samples (at dry and wet states) were clamped in between 2 Plexiglas supports with a 0.5-cm hole in the middle. The test speed was set to 10 mm/min. The maximum load force of the force vs. displacement curve was determined to be the critical penetration force of the sample. Wet samples were wetted with water (2 mL) sprayed in the samples using an air brush.

Modeling Methods. See *SI Appendix*, section 4.

ACKNOWLEDGMENTS. We acknowledge financial support from National Institute of Environmental Health Sciences Superfund Research Program P42 ES013660. D.L., Y.L., and H.G. gratefully acknowledge support from the National Science Foundation (Grant CMMI-1634492). This work was also supported by a graduate fellowship to D.L. from the China Scholarship Council. We acknowledge Dr. David Rand at Brown University for useful technical discussions and Dr. Indrek Külaots for his assistance with graphene materials characterization.

1. E. Singh, M. Meyyappan, H. S. Nalwa, Flexible graphene-based wearable gas and chemical sensors. *ACS Appl. Mater. Interfaces* **9**, 34544–34586 (2017).
2. N. Karim *et al.*, Scalable production of graphene-based wearable E-textiles. *ACS Nano* **11**, 12266–12275 (2017).
3. Y. Wang *et al.*, Wearable and highly sensitive graphene strain sensors for human motion monitoring. *Adv. Funct. Mater.* **24**, 4666–4670 (2014).
4. S. Kabiri Ameri *et al.*, Graphene electronic tattoo sensors. *ACS Nano* **11**, 7634–7641 (2017).
5. L. Qu *et al.*, Functionalization of cotton fabric at low graphene nanoplate content for ultrastrong ultraviolet blocking. *Carbon* **80**, 565–574 (2014).
6. J.-H. Lee, P. E. Loya, J. Lou, E. L. Thomas, Materials science. Dynamic mechanical behavior of multilayer graphene via supersonic projectile penetration. *Science* **346**, 1092–1096 (2014).
7. R. Spitz Steinberg, M. Cruz, N. G. A. Mahfouz, Y. Qiu, R. H. Hurt, Breathable vapor toxicant barriers based on multilayer graphene oxide. *ACS Nano* **11**, 5670–5679 (2017).
8. G. Huang, J. Yang, J. Gao, X. Wang, Thin films of intumescent flame retardant-polyacrylamide and exfoliated graphene oxide fabricated via layer-by-layer assembly for improving flame retardant properties of cotton fabric. *Ind. Eng. Chem. Res.* **51**, 12355–12366 (2012).
9. L. Liu, Y. Yu, C. Yan, K. Li, Z. Zheng, Wearable energy-dense and power-dense supercapacitor yarns enabled by scalable graphene-metallic textile composite electrodes. *Nat. Commun.* **6**, 7260 (2015).
10. P.-Y. Chen, M. Zhang, M. Liu, I. Y. Wong, R. H. Hurt, Ultrastretchable graphene-based molecular barriers for chemical protection, detection, and actuation. *ACS Nano* **12**, 234–244 (2018).
11. C. S. McBride, Genes and odors underlying the recent evolution of mosquito preference for humans. *Curr. Biol.* **26**, R41–R46 (2016).
12. A. J. Shoffstall *et al.*, A mosquito inspired strategy to implant microprobes into the brain. *Sci. Rep.* **8**, 122 (2018).
13. M. K. Ramasubramanian, O. M. Barham, V. Swaminathan, Mechanics of a mosquito bite with applications to microneedle design. *Bioinspir. Biomim.* **3**, 046001 (2008).
14. X. Q. Kong, C. W. Wu, Mosquito proboscis: An elegant biomicroelectromechanical system. *Phys. Rev. E Stat. Nonlin. Soft Matter Phys.* **82**, 011910 (2010).
15. X. Q. Kong, C. W. Wu, Measurement and prediction of insertion force for the mosquito fascicle penetrating into human skin. *J. Bionics Eng.* **6**, 143–152 (2009).
16. C. Lee, X. Wei, J. W. Kysar, J. Hone, Measurement of the elastic properties and intrinsic strength of monolayer graphene. *Science* **321**, 385–388 (2008).
17. C. Cao, M. Daly, C. V. Singh, Y. Sun, T. Filleter, High strength measurement of monolayer graphene oxide. *Carbon* **81**, 497–504 (2015).
18. X. Wei *et al.*, Plasticity and ductility in graphene oxide through a mechanochemically induced damage tolerance mechanism. *Nat. Commun.* **6**, 8029 (2015).
19. J. I. Raji, M. DeGennaro, Genetic analysis of mosquito detection of humans. *Curr. Opin. Insect Sci.* **20**, 34–38 (2017).
20. F. van Breugel, J. Riffell, A. Fairhall, M. H. Dickinson, Mosquitoes use vision to associate odor plumes with thermal targets. *Curr. Biol.* **25**, 2123–2129 (2015).
21. U. R. Bernier, D. L. Kline, C. E. Schreck, R. A. Yost, D. R. Barnard, Chemical analysis of human skin emanations: Comparison of volatiles from humans that differ in attraction of Aedes aegypti (Diptera: Culicidae). *J. Am. Mosq. Control Assoc.* **18**, 186–195 (2002).
22. U. R. Bernier, D. L. Kline, D. R. Barnard, C. E. Schreck, R. A. Yost, Analysis of human skin emanations by gas chromatography/mass spectrometry. 2. Identification of volatile compounds that are candidate attractants for the yellow fever mosquito (Aedes aegypti). *Anal. Chem.* **72**, 747–756 (2000).
23. J. S. Bunch *et al.*, Impermeable atomic membranes from graphene sheets. *Nano Lett.* **8**, 2458–2462 (2008).
24. Y. Su *et al.*, Impermeable barrier films and protective coatings based on reduced graphene oxide. *Nat. Commun.* **5**, 4843 (2014).
25. K. Goh *et al.*, Sandwich-architectured poly(lactic acid)-graphene composite food packaging films. *ACS Appl. Mater. Interfaces* **8**, 9994–10004 (2016).
26. R. R. Nair, H. A. Wu, P. N. Jayaram, I. V. Grigorieva, A. K. Geim, Unimpeded permeation of water through helium-leak-tight graphene-based membranes. *Science* **335**, 442–444 (2012).
27. C. Finlayson, J. Saingamsook, P. Somboon, A simple and affordable membrane-feeding method for Aedes aegpyti and Anopheles minimus (Diptera: Culicidae). *Acta Trop.* **152**, 245–251 (2015).
28. K. K. Gonzales, I. A. Hansen, Artificial diets for mosquitoes. *Int. J. Environ. Res. Public Health* **13**, E1267 (2016).
29. B. Lian *et al.*, Extraordinary water adsorption characteristics of graphene oxide. *Chem. Sci.* **9**, 5106–5111 (2018).
30. M. R. Begley, T. J. Mackin, Spherical indentation of freestanding circular thin films in the membrane regime. *J. Mech. Phys. Solids* **52**, 2005–2023 (2004).
31. U. Komaragiri, M. Begley, J. Simmonds, The mechanical response of freestanding circular elastic films under point and pressure loads. *J. Appl. Mech.* **72**, 203–212 (2005).
32. D. A. Dikin *et al.*, Preparation and characterization of graphene oxide paper. *Nature* **448**, 457–460 (2007).
33. S. Pei, J. Zhao, J. Du, W. Ren, H.-M. Cheng, Direct reduction of graphene oxide films into highly conductive and flexible graphene films by hydrohalic acids. *Carbon* **48**, 4466–4474 (2010).
34. X. Lin *et al.*, Fabrication of highly-aligned, conductive, and strong graphene papers using ultralarge graphene oxide sheets. *ACS Nano* **6**, 10708–10719 (2012).
35. C. Wang, M. D. Frogley, G. Cinque, L.-Q. Liu, A. H. Barber, Deformation and failure mechanisms in graphene oxide paper using in situ nanomechanical tensile testing. *Carbon* **63**, 471–477 (2013).
36. H. Imam, Zarnigar, G. Sofi,A. Seikh,The basic rules and methods of mosquito rearing (*Aedes aegypti*). *Trop. Parasitol.* **4**,53–55 (2014).